Numerical Investigation of the Behavior of MERO Joint System Under Combined Loading Regarding Helical Threads of Elements

Mehdi Ebadi Jamkhaneh, Amir Homaioon Ebrahimi & Maedeh Shokri Amiri

International Journal of Steel Structures

ISSN 1598-2351

Int J Steel Struct
DOI 10.1007/s13296-020-00330-8

Springer

International Journal of Steel Structures
https://doi.org/10.1007/s13296-020-00330-8

Online ISSN 2093-6311
Print ISSN 1598-2351

Numerical Investigation of the Behavior of MERO Joint System Under Combined Loading Regarding Helical Threads of Elements

Mehdi Ebadi Jamkhaneh[1] · Amir Homaioon Ebrahimi[2] · Maedeh Shokri Amiri[3]

Received: 6 August 2019 / Accepted: 19 March 2020

Abstract
A comprehensive finite element (FE) model of bolt-ball joint, as called MERO joint, is presented in this paper for a double layer grid structure. In double layer grids, the main internal forces are axial forces. The deflection and rotation patterns of the connector are studied under different loading conditions using the ABAQUS FE software. The applied forces on the connector are determined using displacement control. In order to take into account the connector effects in structural analysis, their behavior under combined loading should be predicted. To determine the load–displacement relationship of the MERO connection, numerical models were carried out on a connector of this type using of 3D FE method. The obtained load–displacement and moment- rotation relationships were used under different loads. The results of the FE simulation with experimental results have a good match. Compressive axial load increases the flexural stiffness of the connection and decreases the elastic bending moment. Furthermore, the equivalent stiffness of bolt with the whole of complexities was proposed.

Keywords Bolt-ball joint · Nonlinear finite element method · Bending moment loading · Load–displacement behavior · Elastic stiffness

1 Introduction

The bolt-ball (BB) joint is one of the most common joints used to make double/multilayer grids. Previous studies conducted on structures constructed using such system indicate that responses resulted from the analysis without considering joint effect have a significant difference to real responses of the same. Therefore, to find more realistic analysis results, the joint effect shall be considered in the analysis of the structure. In static analysis, double/multilayer grids under loads applied on nodes is the dominant axial force and other forces and moments have the secondary roles. In order to include the effect of joints in structures on the static analysis, it is enough to determine their load-axial displacement relationship. The existence of different elements of joint together with pre-stress resulted from tightening the bolt and spiral nature of thread intensify joint behavior complexity. Notably, in conducted studies in the field of modeling joint with bolt and thread, the proposed models have several simplifications and sometimes ignore the effect of the threaded spiral. Vaseghi Amiri and Davoodi (2002) made a double layer grid with the BB joint in full scale. They assessed the force–displacement relationship of some nodes of the grid due to applying a concentrated load. Their results indicated that the structure analytical response without considering the effect of joint has a significant difference with their real responses. They also understood that bolts tightening levels affect grid behavior. Davoodi et al. (2007) conducted an experimental study on the same grid and showed that BB joint behavior and its bolt tightening level profoundly effect the grid dynamic responses. Davoodi et al. (2012) used the updating technique of the finite element (FE) model to find the load–displacement relationship of a BB node at the double layer grid. In this study, they used structure response and inverse problem method to find mechanical characteristics of the elements and their behavior. Therefore, the thread effect in bolt and ball has been ignored. Results of this study demonstrated that joint load–displacement relationship in grid includes two parts: the first part, which is related to

✉ Mehdi Ebadi Jamkhaneh
m.ebadi@du.ac.ir

[1] School of Engineering, Damghan University, Damghan, Iran

[2] Department of Civil Engineering, Birmingham University, Birmingham, UK

[3] Urban Planning, Islamic Azad University of Tehran Science and Research Branch, Tehran, Iran

Published online: 27 March 2020

early stages of loading and is nonlinear with positive section. This part indicates early looseness and is the main cause of major uncertainties in the joint. The second part has a higher stiffness with respect to the first part and has almost the same joint behavior separately. Determining the first part of the load–displacement curve of a BB joint at a double layer grid is merely possible through studying joint behavior at a structure due to different uncertainties. The second part of the load–displacement curve may be determined through studying a separate joint, either experimentally or numerically. Previous studies conducted at the University of Cambridge by See and McConnel (1986) indicate that the behavior of a double layer grid with hinge joints has a different behavior with the same structure with the rigid joints. Meanwhile, Fathelbab (1987, 1993) showed that joint stiffness highly affects force–displacement behavior. Therefore, to find more precise results of the analysis, the effect of a joint in an analysis of structure shall be considered. Ebadi Jamkhaneh and Davoodi (2012) and Ebadi Jamkhaneh et al. (2017) studied the effect of the level of MERO joint bolts tightening on tensile and compressive axial behavior. Maalek (1999) suggested test results with single and double axial loading on San Niami ball nodes, which provided new behavioral information regarding the flexibility of such type of links.

El-sheikh (1993) and Chenaghlou et al. (2014) understood that general structure behavior and failure modes are affected by joint bending stiffness. Chenaghlou (1997) found out that compressive axial force highly affected moment-rotation behavior parameters of a MERO joint and suggested a mathematical model of the moment-rotation behavior. Ueki et al. (1993) showed that joint rigidity increases under constant compressive force and decreases under a fixed tensile force. Fan et al. (2012) conducted an experiment on two socket and bolt-ball joints under bending moment, with and without applying axial force. Their study results revealed that the socket and BB joint systems had proper bending stiffness. Mathurin et al. (2009) suggested a three-dimensional (3D) model of the bolt with thread and applied tightening moment to the same. Chen and Shih (1999) conducted a series of studies using the FE method (FEM) on the bolt joint. In these models, effects of friction and direction angle of threads were studied on load distribution at each thread. Ghasemi et al. (2010) conducted an experiment on a separate BB joint and found the load–displacement relationships under tensile loading and different tightening levels. Zeng et al. (2019) studied joint compressive load-bearing capacity, including the bolt and cylindrical ball and Yuan et al. (2019) studied MERO joint load-bearing capacity considering corrosion in bolt threads. Guo et al. (2016a, b) conducted an experimental and numerical study on joints, including bolt and cylindrical ball. They found that the dimensions and cylinder and tube highly affect joint mechanical behavior. ADEOTI et al. (2019) investigated the behavior of semi-rigid aluminium joint as an experimental and numerical models under bending moment load. Their results led to present a bending moment-rotation relationship which is the input data in analytical programs. Cao et al. (2016) assessed the ball joint behavior of one layer dome with the diameter of 80 m. They proposed the bending moment-rotation relationship and conducted the non-linear stability analysis in different level of construction.

Based on the few studies on the MERO joint in determining the force–displacement behavior, a comprehensive FE study is performed in this study. Numerical studies on this joint have neglected the effect of threads on the bolt and ball, which this led to the differences between the results of the force–displacement behavior. On the other hand, some limited tensile or bending loads were considered in the studies. In this study, different types of loading including compressive, tensile, and bending moment loading and the combination of them are applied to the joint for confirmation of the semi-rigid behavior of the joint. Furthermore, a simple analytical model for predicting the connection behavior is presented. Numerical simulation of the thread shape and different parts of the joint are modeled by using Solidworks software and analysis has been completed by using ABAQUS FE software. Considering the analysis of the internal load distribution based on the simulation of the threads, transmission systems were established. The load–displacement relationship of the BB joint has been found under tensile and compression using the numerical method and relevant numerical results were compared with available experimental data. After verification of simulated models, the model is subjected to combined loading and its behavior is studied.

2 Introducing MERO Joint System

MERO joint system is a multi-axial system, to which up to 18 tube members may enter. This system is composed of tube elements, joining at a node using the MERO joint system. Other members of this system are composed of threaded steel ball, conic parts, wrenching sleeve, and threaded bolt together with the joint pin, which is used to joint bolt and sleeve. Opening on the sleeve enables joint pin handling. Interaction between tube elements and joints in the double layer grids often includes tensile and compression effects. Tensile in tube element is transmitted to the ball by conic end piece and through bolt, in which case the bolt is under tensile and sleeve is inactive. Compression force in the element is transmitted to ball through conic end piece and sleeve. Joint elements with meshed model and the elements sizes have been given in Fig. 1.

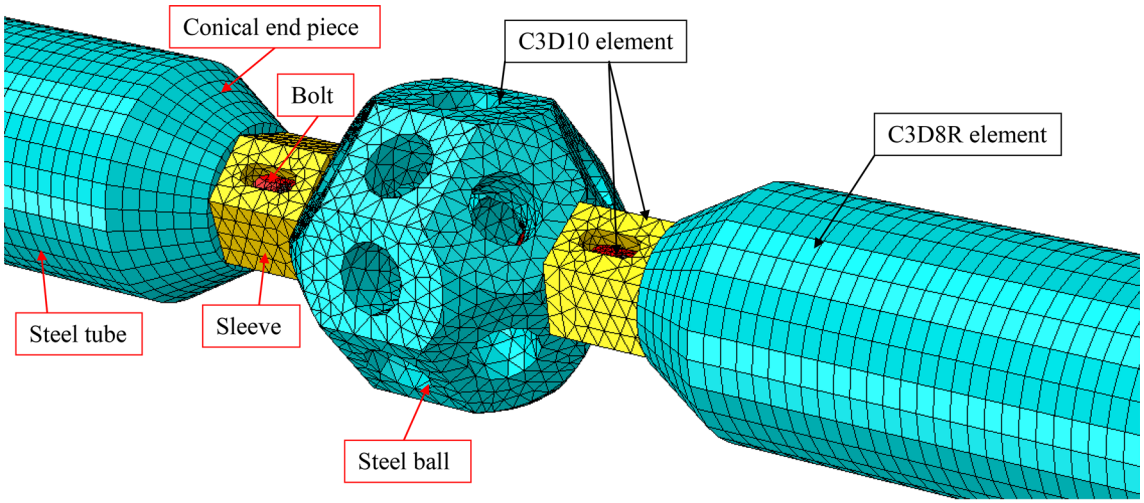

(a) Details and mesh of the ball joint system

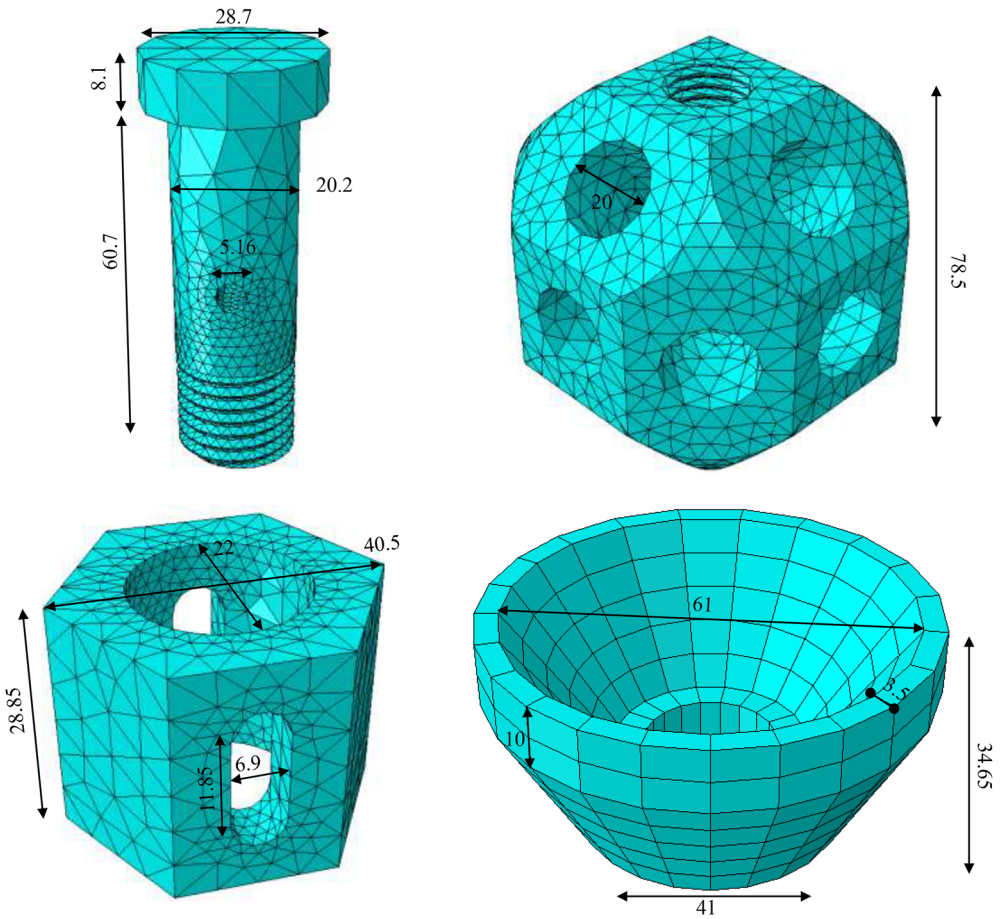

(b) Dimensions and mesh sizes of MERO joint parts

Fig. 1 Introducing of meshed MERO joint and dimensions of its components

3 Finite Element Modeling of MERO Joint

During recent years, finite element (FE) simulation has significantly become popular due to the advancement of computer technology and numerical models. Eventually, numerical methods are suitable for certain simulation processes, e.g., materials forming operations, rolling, and complex geometrical shapes, as they are precise and

decrease calculation time. Numerical simulation of thread shape and different parts presented in this study have been completed using Solidworks software and analysis has been conducted by ABAQUS/standard FE software.

3.1 Material Properties

To model steel materials features of the joint members, multi-linear elastic–plastic behavior with von Mises yield criterion and dependent flow law have been used. Nominal stress versus strain curves were obtained from coupon tests (by Ghasemi (2007)) and converted into the true stress–strain form to account for material nonlinearity:

$$\sigma_{true} = \sigma_e \left(1 + \varepsilon_e\right) \tag{1}$$

$$\varepsilon_{true} = \ln \left(1 + \varepsilon_e\right) \tag{2}$$

where σ_{true}, σ_e, ε_e and ε_{true} are the true stress, nominal stress, true strain, and nominal strain, respectively. Kinematic hardening was used to simulate the material's post-yield behavior with its moving yield surface property (ABAQUS Users' Manual). The true stress–strain relation is given in Fig. 2. For all steel materials, the value of elastic modulus and Poisson's ratio were 200,000 MPa and 0.3 respectively. Based on the conducted experiments by Ghasemi (2007), high strength bolt of 800 MPa was used in the specimens. The true yield and ultimate stresses of conical end piece and sleeve were found to be 300 MPa and 490 MPa, respectively. Material properties of steel spherical ball, with yield stress of 240 MPa and others are shown in Fig. 2, which were determined based on the model adopted by Ghasemi (2007).

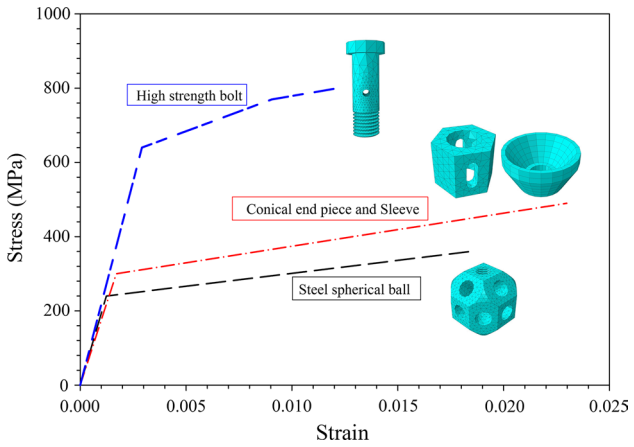

Fig. 2 Stress–strain relationships of the MERO joint parts (Ghasemi et al. 2010; Ghasemi 2007)

3.2 Element Selection

Meshing algorithm is referred to as a set of techniques to develop a regular and practical finite elements grid on the geometrical model. For all elements except conic, free mesh technique with tetrahedral shape has been applied. Using wedge elements, a border layer was defined along relevant model border surfaces. This border layer includes a set of wedge elements with a normal vector perpendicular to a solid surface wall with minimum thickness. The preceding algorithm develops a compact grid of wedge elements at the border region and with less intense at the middle of the body (tetrahedral elements location). For the conic part, meshing with hexahedral elements using sweep technique has been used. Finally, compatibility meshing was conducted using the ALEABAQUS method to compare with big deformation at thread location to improve solution accuracy at the thread location. Bolt, sleeve, and ball as the discrete parts, have been modeled with C3D10 element, tetrahedral, 3D, 10-node elements, and continuous environment. Conic end piece has been modeled as C3D8R with hexahedral, 3D, 8-node elements, and using reduced integration. Number of C3D10 and C3D8R elements equal to 59,610 and 5766, respectively. These elements have been shown in Fig. 1. The size of elements in thread regions was taken finer than other parts due to keeping geometry and proper output results from other parts.

3.3 Modeling of Interaction Between Parts

One of the challenging aspects of this study is successful modeling contact between different joint parts with a contact algorithm. They allow the forces to transmit from one part of the model to another as long as surfaces are in contact with each other. When the surfaces detach, no constraint is applied. Contact pair algorithm in ABAQUS/standard was used to model the interaction between different parts of joint (conic and bolt, conic and sleeve, sleeve and ball, bolt and ball). First of all, two contact surfaces are defined geometrically. One of the surfaces is considered as master and the other as slave. Until the two surfaces contact each other, shear and normal forces are transmitted along the normal surface. However, tensile bonding between contact surfaces is considered to be zero. A mechanical interaction model, including friction, is defined for the contact model between surfaces. Coulomb base friction model was used in ABAQUS for the formulation of normal and tangent forces using friction coefficient (Ebadi Jamkhaneh et al. 2020). Under all contact states, 0.14 as a friction coefficient and hard contact were utilized. Under such a case, elements do not penetrate into each other and joint elements (sleeve and conic) may separate under tensile loads. In order to remove the intervention of geometrical volumes in thread regions,

the smoothing method in the interaction section has been used.

3.4 Boundary Conditions and Loading Protocol

Two types of axial and bending moment loading were conducted on the joint. In axial loading, two types of pure axial compression and tensile loads were applied to the joint. To do so, support boundary conditions were considered differently in proportion to the type of loading. Under axial loading, the ending surface of one of the conics was bounded through applying restraint along the joint longitudinal axis. Applying force was made through the ending surface of the other conic. Under bending moment loading, the two ends of the tube (as per Fig. 3) were controlled by hinged support and load was applied to nodes in the middle of the steel ball. Loading was considered as a monotonic type using the displacement control method.

4 Numerical Verification

Numerical model validation was made in two stages. In the first stage, the simulated numerical model was verified utilizing a joint experimental sample. In the second stage, validation was conducted by focusing on bolt threads and ball from another reference.

First Stage

According to Fig. 4, the joint sample was exposed to tensile load and the joint axial load–displacement behavior was extracted. In Fig. 5, a comparison has been conducted among experimental and FEM results. Through comparing the behavior of the two samples, it was understood that the initial elastic stiffness of experimental and numerical models is equal to 184 and 191 kN/mm, respectively. In other words, elastic stiffness resulted from the numerical model analysis is almost 4% larger than that of an experimental sample. Under tensile load, bolt plays a major role in force transmission mechanism, and the sleeve has no role in such a mechanism. In Fig. 6, the sequence of failure mechanism and stress distribution have been shown for the bolt.

Stress concentration is more focused on gap and threads regions where there are big openings and less cross-section. According to the previous studies (Serway and Beichner 2000), the first three threads have the biggest portion of axial force absorption, which has well been indicated in Fig. 7. In this figure, the surrounding of the hole shows high-stress concentration due to less cross-section at the bolt body hole location. Under pure tensile load, opening a location in the bolt, joint ending cone outer edge, and first thread, as well as

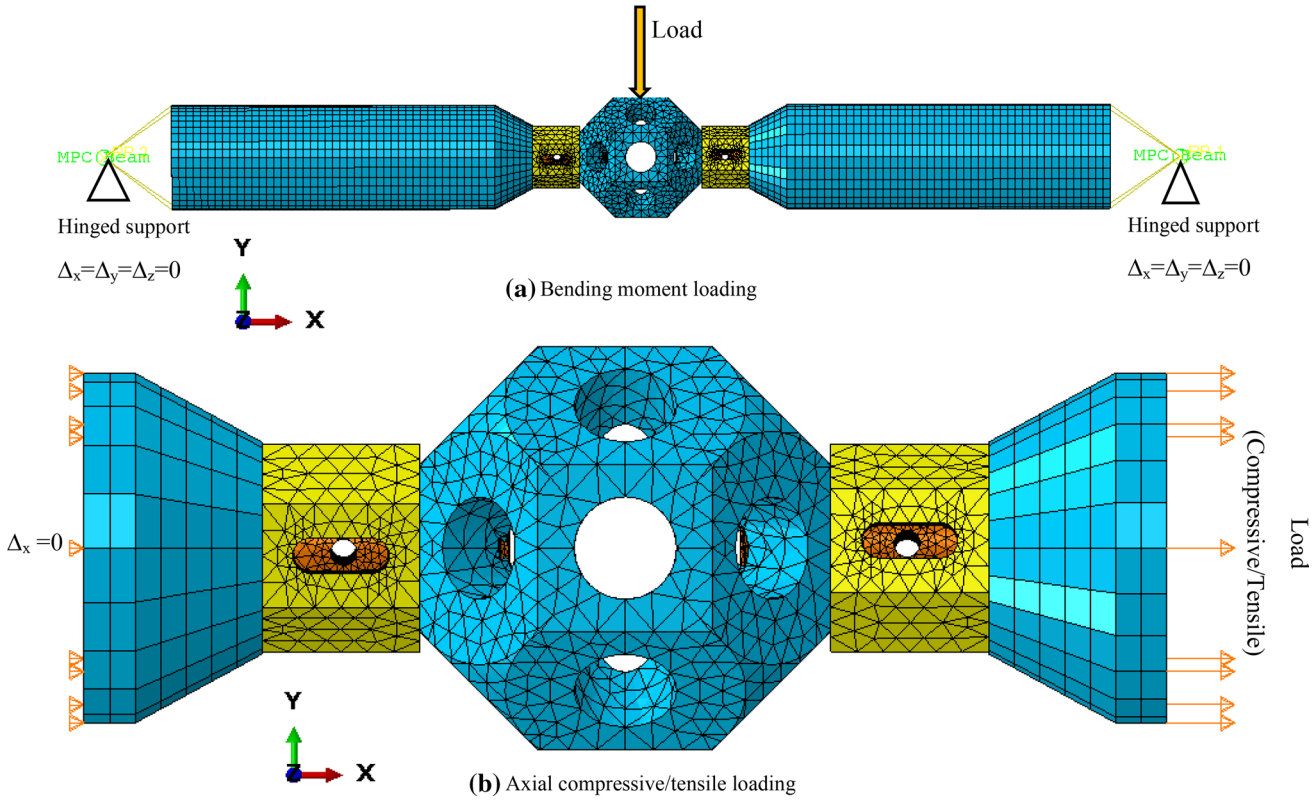

Fig. 3 Applying boundary conditions and loading types

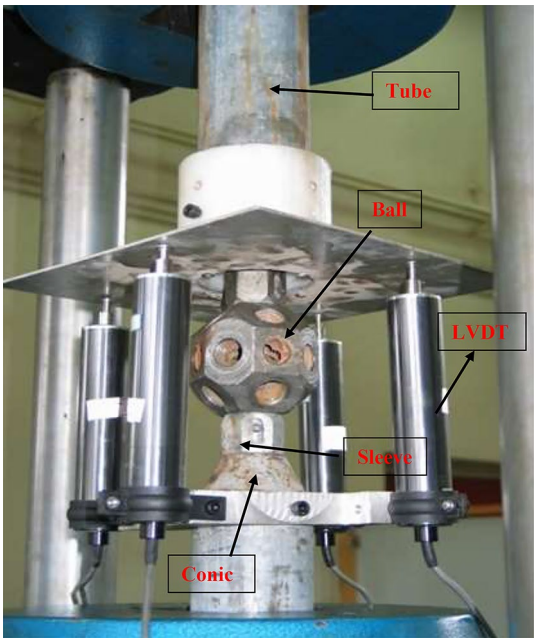

Fig. 4 Experimental test of MERO joint under tensile loading

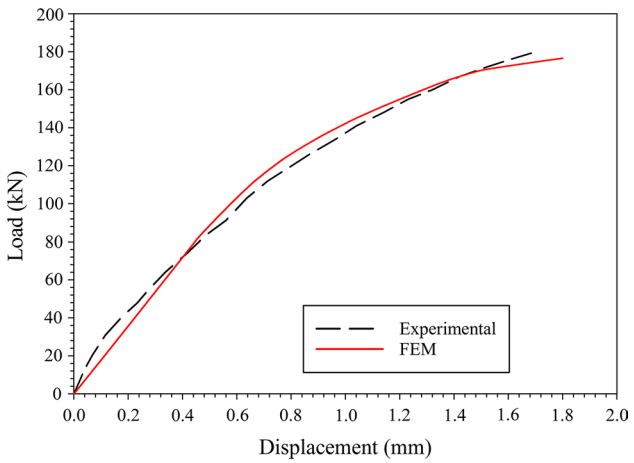

Fig. 5 Comparison of load–displacement curves of tested specimen and FEM results

certain parts of ball with little thickness, were yielded faster. According to Fig. 7, the first three threads of the bolt which are in contact with bolt threads tolerate almost 70% out of tensile, while the first thread has tolerated almost 33% out of total applied tensile (55.8 kN).

Second Stage

FEM was conducted on 8UNC bolt using ABAQUS software to determine load distribution percentage on the thread based on a reference model (Chen and Shih 1999). In these models, the boundary conditions, including loading and supporting conditions, are similar. In these models, an axial load is applied to the top part of the bolt. According to the unknown nature of loading type, rigid plane was used for applying the concentrated/uniform load. Uniform load is applied to rigid surface of the bolt ending (Fig. 8). In Fig. 9, a comparison was conducted between Chen and Shih (1999) modeling results. As it is observed, a little difference (roughly 2% in first thread) between two models demonstrates proper accuracy in modeling with reference.

Considering the results, the same method (using uniform load to apply tensile and compression loads, taking benefit from a rigid surface at the end of conic to achieve displacement, and types of elements used in thread) have been used.

5 Results and Discussion

5.1 Joint Behavior Under Compressive Loading

In the tensile transmission state, bolt plays the main role for axial force transmission mechanism, while sleeve plays such a role in case of applying a compressive force to the joint. Therefore, It cannot properly predict the behavior in compressive load because of the different roles of members in the force transmission mechanism. The intricate behavior of the MERO joint under tensile load was due to the threads of the bolt and ball node. Therefore, this model can be used for the compressive loading, which even has no thread and complicated cased in this type of loading. Figure 10 shows the compressive load-axial displacement relationship of the joint. It is seen through comparing among joint members and the whole joint in Fig. 10 that the conic end piece has yielded faster. In the compressive force transmission system, a bolt was taken out of the system and the bolt transmitted no force. In Fig. 11, effective stress of the conic has been shown under a pure compressive state in the stage of joint yielding and end of loading. Notably, the results given in the figures depend on the type of materials and sample dimensions. On the other hand, by modeling two joint samples under tensile and compressive loading, it is considered as a certain type of similar joints with size similarity.

The ball threaded zones, external edge of the ending cone, and opening edges of the sleeve with fewer cross-sections yielded faster under the compressive state. The blue colored zones in sleeve demonstrate such zones were not in contact with the ball and the upper blue colored ones (quite limited stress areas) of the sleeve show that there is no contact surface between the sleeve and bolt under compression.

5.2 Joint Behavior Under Bending Moment Loading

Mechanical behavior of the joints may be expressed as a moment-rotation curve, indicating the relation between applied bending moment and respective rotation. The bending moment applied to the joint equals support force

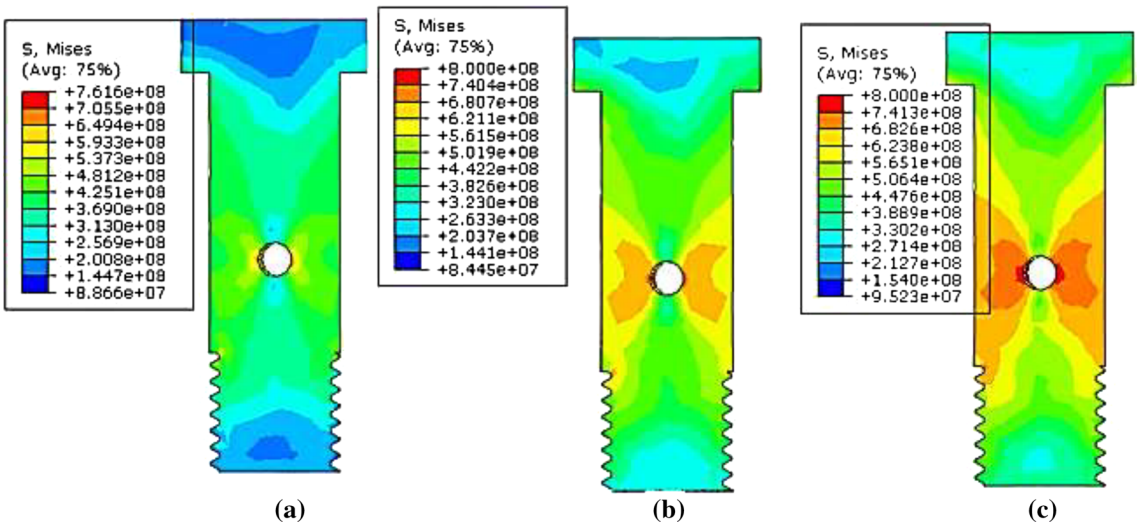

Fig. 6 Sequences of failure mode of the bolt; **a** displacement at 0.4 mm, **b** displacement at 1.0 mm, and **c** displacement at 1.7 mm

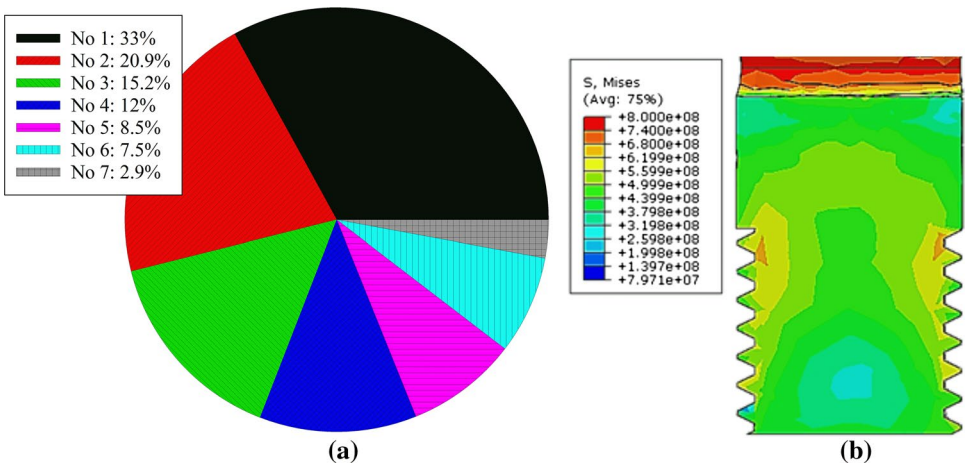

Fig. 7 Distribution of tensile load; **a** percentage of tolerated tensile load on threads of bolt and **b** stress distribution on bolt

along a tube, as shown in Fig. 12a. On the other hand, rotation deformation is equal to the total elastic deformation of the tube and rotation deformation of the connection.

$$\emptyset = \frac{\sum_{k=1}^{n} \emptyset_{ij}}{n} \tag{3}$$

$$\emptyset_{ij} = \arctan\left(\frac{\delta_i - \delta_j}{l_{ij}}\right) \tag{4}$$

where δ_i and δ_j are deformations measured at the beginning of the tube and the ball. L_{ij} denotes the distance between these two points. Initial bending stiffness, resisting moment, and rotation capacity of the joint may be found using bending moment- rotation curve (Fig. 12b) (Girão Coelho et al. 2006).

The midpoint of the tube circular cross-section at the beginning and center point of ball drilled surfaces is used in order to determine the rotation. By calculating extracted displacement in proportion to loading direction and dividing the difference of these two by length, rotation can be estimated. In this study, the elastic deformation of the tube is quite limited (around 1%), which is ignorable comparing to joint deformation. Therefore, rotation deformation roughly equals joint deformation. In Fig. 12b, the tangent line on A point has a slope called initial bending stiffness. The tangent line on B point has a less slope, which is reduced stiffness. This stiffness is about 20% of initial bending stiffness. Therefore, moments associated with A and B points are called elastic and plastic moments. Knee-range is a range between initial and reduced stiffness and reaches (M_{inf} and Φ_{inf}) from the lower part and (M_{sup} and Φ_{sup}) from the upper part. The

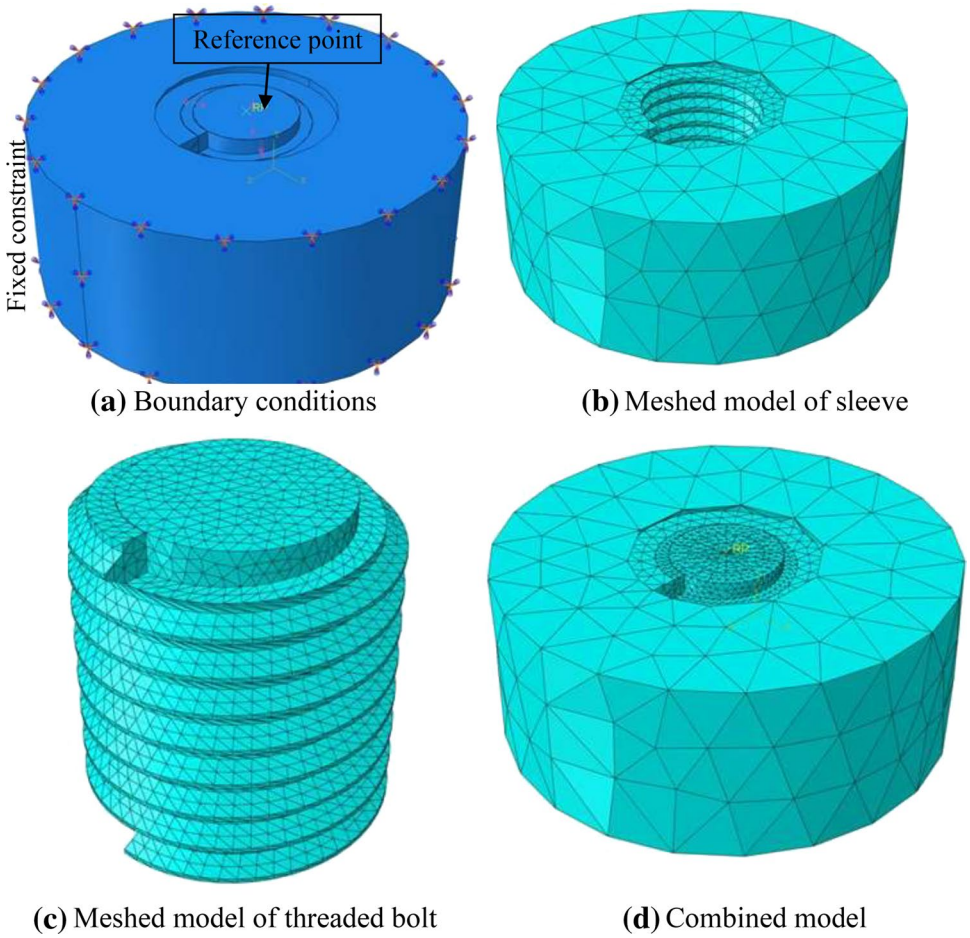

Fig. 8 Modeling of threads and boundary conditions

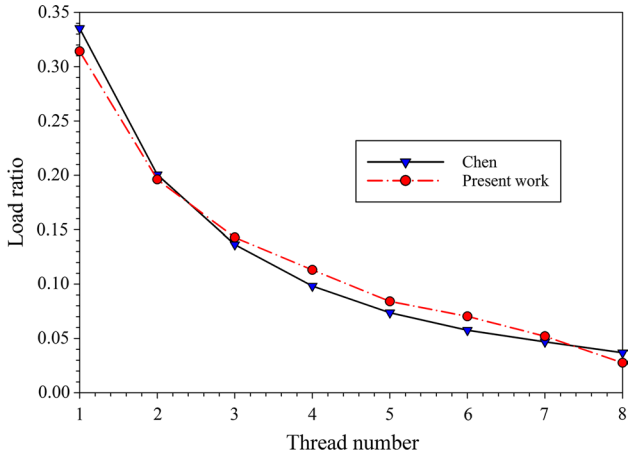

Fig. 9 Comparison of load ratio between Chen and Shih model and FEM model

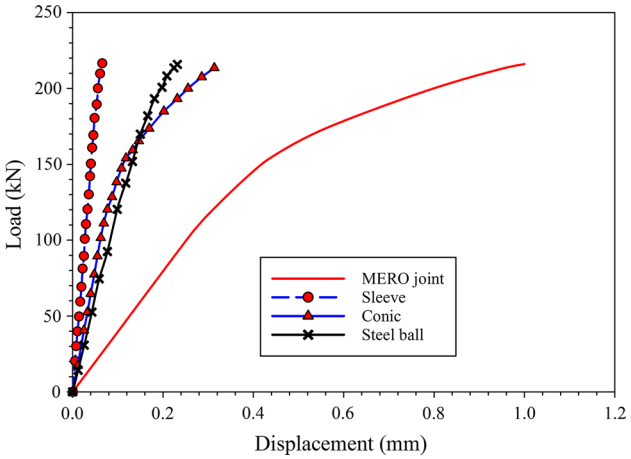

Fig. 10 Portion of each parts of joint under compressive load

loading procedure is in the form of displacement control to the top of the ball and monotonic type. Figure 13 shows the deformed connection under bending moment loading.

As a result of the bending moment, the top part of the sleeve is compressed, and its bottom part is under tensile. Upon the presence of the positive bending moment, it is expected that the top and bottom parts of the bolt are subjected to compression and tensile loads, respectively. Upon applying a load, the upper and lower parts of the ball node are exposed to compression and tensile, respectively. Furthermore, the threaded hole of the ball imposes compression

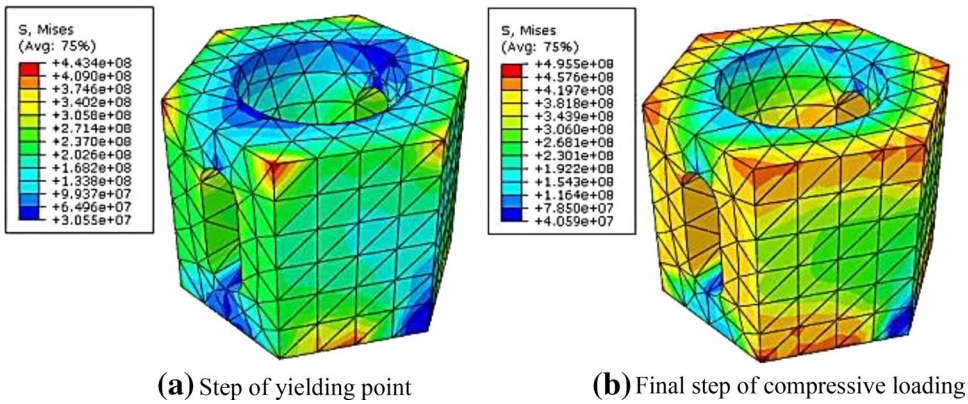

(a) Step of yielding point **(b)** Final step of compressive loading

Fig. 11 Stress distribution on sleeve in two steps

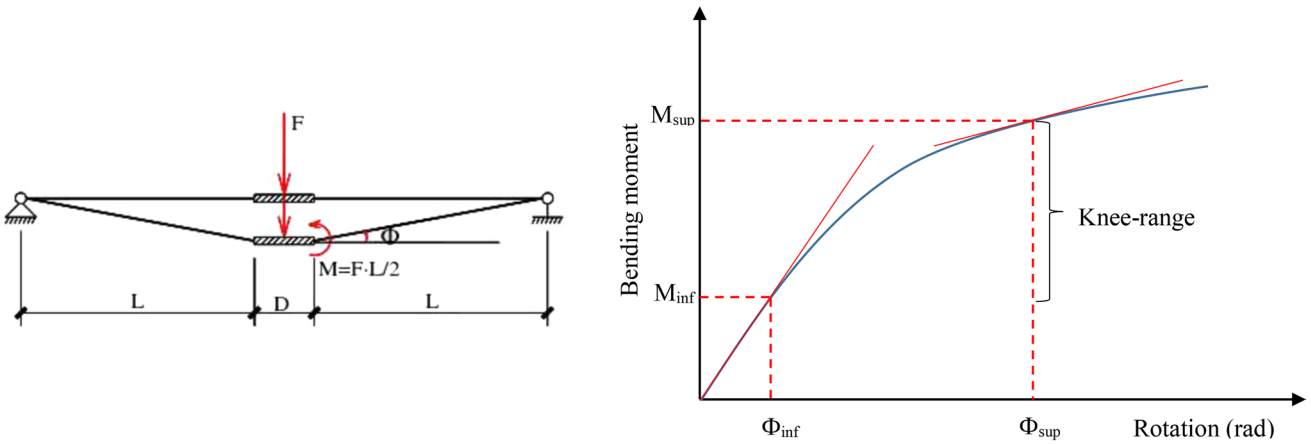

(a) Applying a bending moment loading **(b)** Bending moment-rotation curve

Fig. 12 Definition of bending moment-rotation relationship

resulted from opening to bolt lower parts, which results in compression stresses on the bolt. In Fig. 13, half of the joint section cut has been shown for more clarification. Under bending moment loading, the connection had a plastic deformation. In Fig. 14, the bending moment- rotation curve has been given.

5.3 Joint Behavior Under Combined Loading

In fact, a combination of loads may impose a joint system. Therefore, here we focus the combined effect of compressive force and bending moment loads. Considering Fig. 15, rotation of the joint and bending moment measurements may be calculated.

Two compressive force and bending moment loading were applied to the model using the displacement control method. In both cases, lateral displacement loading for 25 mm has been applied. In the first model, the displacement denoting applying compression reaches 1 mm and in the second mode, it was limited to 2 mm, to observe the compression load effect in joint behavior. On the other hand, the effect of lateral and compressive loadings, a developed gap between sleeve and ball, and compressive force applied to the bolt threads may be understood. In Fig. 16, bending moment-rotation curve has been given. Simultaneous applying compression force and bending moment results in an increase in initial bending stiffness. This is due to that it is delayed by applying compressive force with bending moment, detaching joint parts, and creating a gap between them. The existence of gaps between parts results in a decrease in the knee-range.

5.4 Joint Analytical Relations

It may be found out considering tensile loading capacity calculations of each part of the joint that the maximum load applied to the joint system is equal to 173.1 kN, which is the same as bolt failure force at the hole section. It is seen under compressive loading that as exposed to 146.81 kN force, the sleeve enters into a nonlinear stage, and the maximum

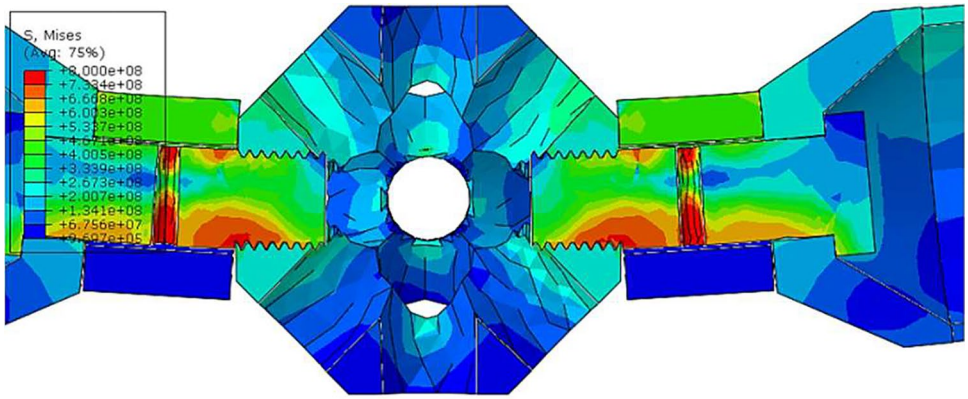

Fig. 13 Deformed shape of joint under bending moment load

force which may be applied to the joint system is equal to 226.3 kN, which is equal to yielding force of the sleeve in hole section.

In order to draw the analytical relationship of the joint system load–displacement, joint displacement was considered equal to total bolt, conic, and ball deformations. By using load–displacement presented for the bolt and conic, the displacement respective to applied force can be determined. Roughly ball displacement is taken as equal to 10% of the total bolt and conic displacements. The reason for displacements doubling is the existence of two bolts and two conics in the joint. Considering joint load–displacement analytical curve data has been given in Fig. 17.

Bolt tensile stiffness in its elastic behavior section is more significant than the MERO joint model. On the other hand, the nonlinear behavior of the bolt model with respect to the joint element model occurs in a similar range of load. By determining the manually axial stiffness of the bolt, the FE analysis of the joint model results may be controlled (Fig. 18). In the analytical method, the bolt may be classified into three parts of the bolt head, bold body, and threaded part.

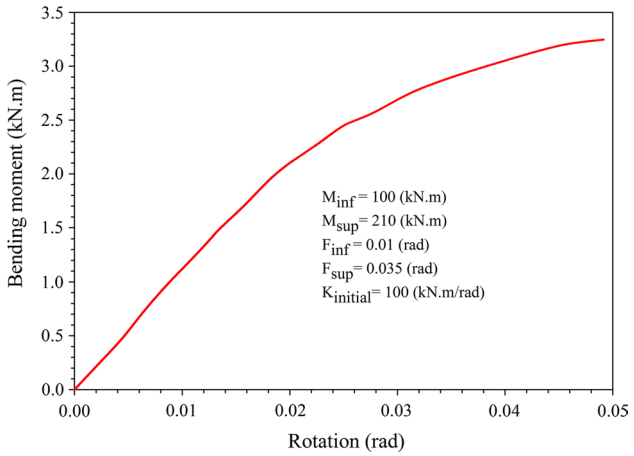

Fig. 14 Bending moment-rotation curve of MERO joint

These three parts may be equalized with three cylindrical sections along with each other, like series springs. Therefore, the stiffness of each of these cylinders is found suing EA/L formula. Therefore, equivalent stiffness of bolt in this method can be found using the following relation:

$$\frac{1}{k_{e(bolt)}} = \frac{1}{k_1} + \frac{1}{k_2} + \frac{1}{k_3} \rightarrow k_{e(bolt)} = 1013.2 \text{ (kN/mm)} \quad (5)$$

Evidently, in such an equalizing method, the hole on the bolt body has been ignored. According to Fig. 18, bolt model results indicate its tensile stiffness to be within its elastic behavior range (785.2 kN/mm). (Displacement values on bolt stiffness curve in Fig. 18 are halved). Therefore, analytical relation shows a 25% difference in comparison to the foregoing. According to the presumption considered in calculations of bolt stiffness, such difference may be interpreted as ignoring the role of a hole on bolt body for its axial stiffness reduction. Therefore, it may be concluded that by a 25% decrease of axial stiffness resulted from analytical calculations using series springs, the error can be limited, and the real value of bolt tensile stiffness can be approached. As seen in Fig. 18, the bolt nonlinear behavior commences from a lower range of load. Commencement of joint nonlinear behavior in tensile axial load is more affected by bolt behavior. It indicates that nonlinear behavior in the joint model starts from the bolt.

6 Conclusions

In this study, MERO joint behavior was studied using the FEM in the ABAQUS program under pure tensile, pure compression, bending moment, and a combination of those loads. Joint behavior was presented in the form of axial load–displacement and bending moment-rotation curves. The following conclusions can be made based on the investigation.

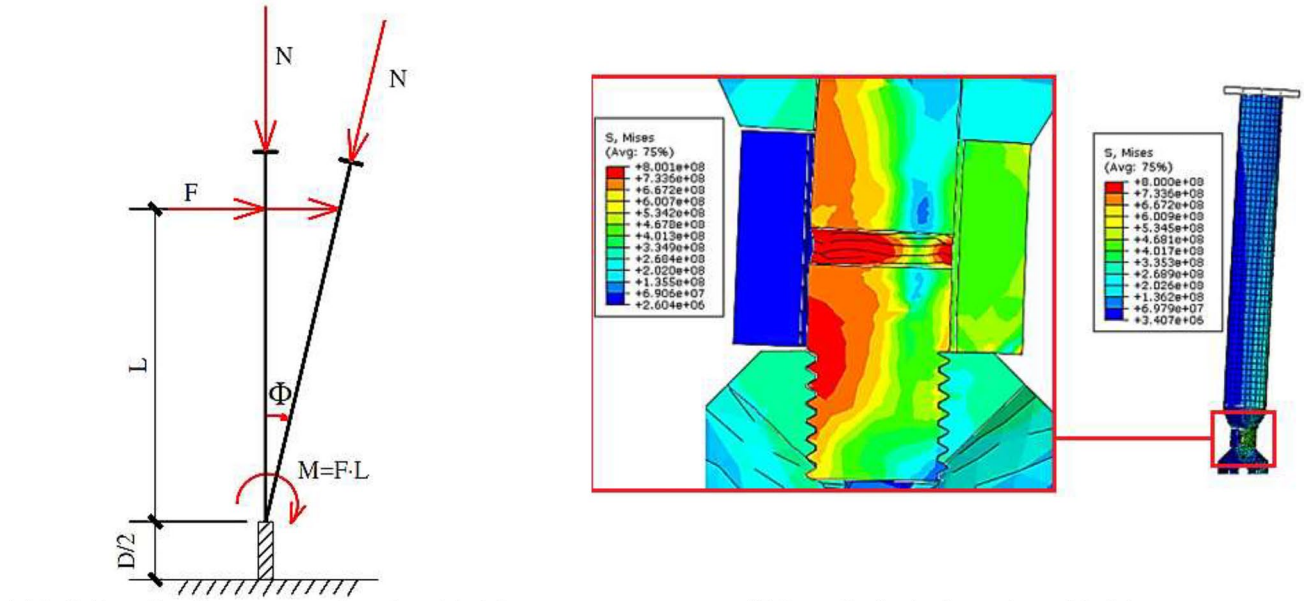

(a) Definition of bending moment and rotation of the joint

(b) Stress distribution in members of the joint

Fig. 15 Definition of combined loading and stress distribution on different parts

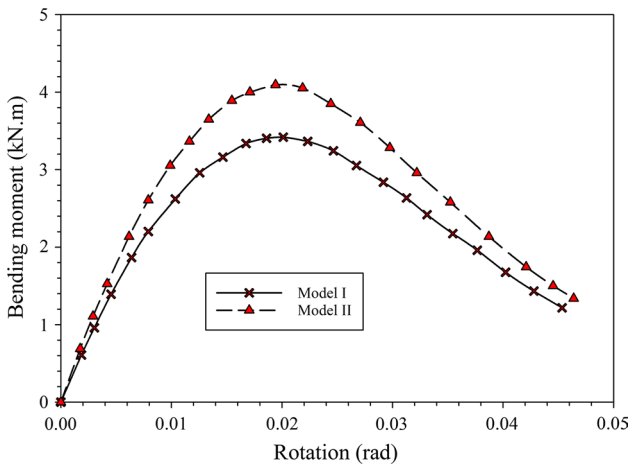

Fig. 16 Bending moment-rotation curves related two states of loading

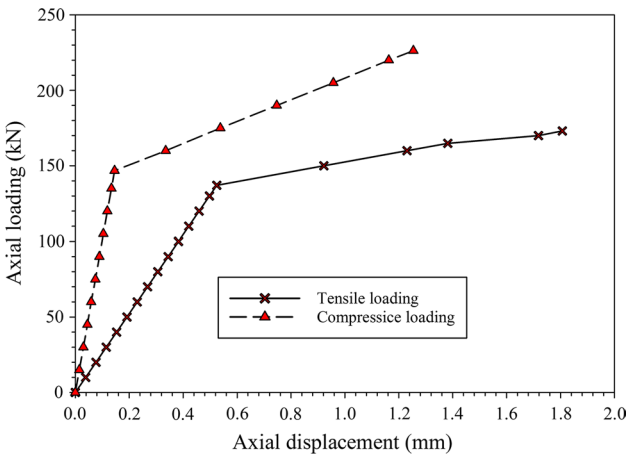

Fig. 17 Analytical load–displacement curves of joint under tensile and compression loads

- Under pure tensile load, the joint has an elastic level up to 112 kN and then enters into a nonlinear zone. In this case, the opening region on the bolt and first thread of the ball reached to failure stage.
- Under pure compressive force, the joint has an elastic stage up to 135 kN. Then it enters into a nonlinear stage upon conic yielding. The initial stiffness of the joint under compression loading is 1.81 times that of joint stiffness under tensile exposure.
- The compressive axial force increases joint initial bending stiffness. Meanwhile, the elastic bending moment decreases by increasing compressive force.
- In the case of using analytical relation, joint elastic stiffness becomes roughly 25% larger than the stiffness of FE model, which may be referred to simplifying assumptions such as ignoring hole in bolts.
- Quantitative results presented in this study may merely be referred to concerning the studied model and further studies are required for other standard aspects of MERO joints.

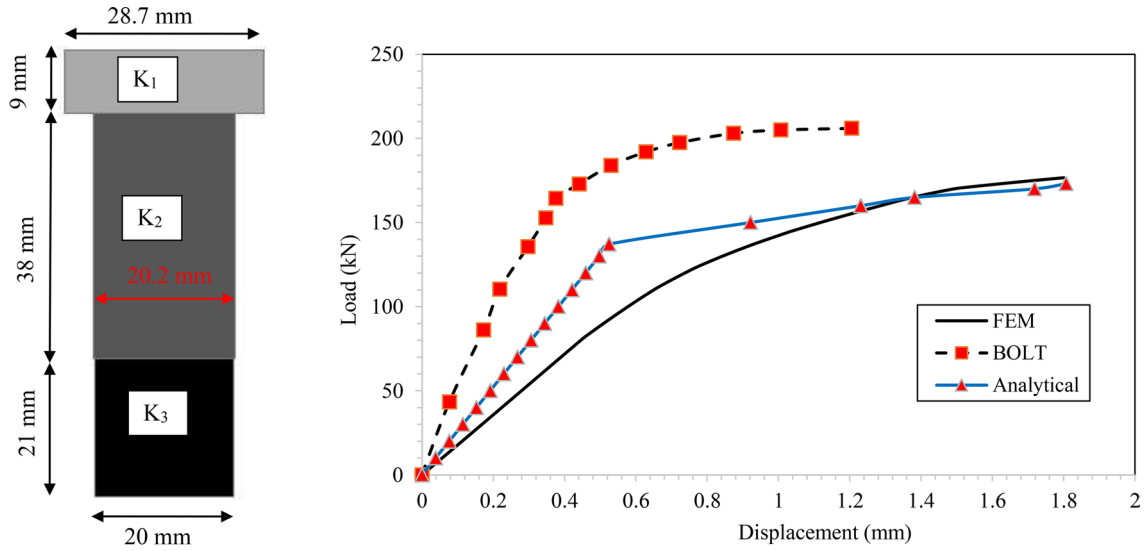

(a) Equvalent stiffness of the bolt

(b) Comparison of the load-displacement curves of FEM and analytical

Fig. 18 Equivalent axial stiffness of bolt and comparison of analytical and FEM model results

References

ABAQUS Standard User's Manual The Abaqus Software is a product of Dassault Systèmes Simulia Corp., Providence, RI, USA Dassault Systèmes, Version 6.14.2, USA (2014).

ADEOTI, G. O., Fan, F., Huihuan, M. A., & Shen, S. (2019). Investigation of aluminium bolted joint (HBJ) system behavior. *Thin-Walled Structures, 144,* 106100.

Cao, Z., Du, P., Chen, Z., & Wan, Z. (2016). The stability and stressed skin effect analyses of an 80 m diameter single-layer latticed dome with bolt-ball joints. *International Journal of Steel Structures, 16*(2), 279–288.

Chen, J. J., & Shih, Y. S. (1999). A study of the helical effect on the thread connection by three dimensional finite element analysis. *Nuclear Engineering and Design, 191*(2), 109–116.

Chenaghlou, M. R. (1997). *Semi-rigidity of connections in space structures*. Ph.D. thesis, University of Surrey.

Chenaghlou, M. R., Nooshin, H., & Harding, J. E. (2014). Proposed mathematical model for semi-rigid joint behaviour (M-θ) in space structures. *International Journal of Space Structures, 29*(2), 71–80.

Davoodi, M. R., Pashaei, M. H., & Mostafavian, S. A. (2007). Experimental study of the effects of bolt tightness on the behaviour of MERO-type double layer grids. *Journal of the International Association for Shell and Spatial Structures, 48*(1), 45–52.

Davoodi, M. R., Vaseghi Amiri, J., Gholampour, S., & Mostafavian, S. A. (2012). Determination of nonlinear behavior of a ball joint system by model updating. *Journal of Constructional Steel Research, 71,* 52–62.

Ebadi Jamkhaneh, M., Ahmadi, M., & Sadeghian, P. (2020). Simplified relations for confinement factors of partially and highly confined areas of concrete in partially encased composite columns. *Engineering Structures, 208,* 110303.

Ebadi Jamkhaneh, M., & Davoodi, M. R. (2012). Evaluate axial stiffness of the MERO connection, under the effect of hardening the screw. *International Journal of Science and Emerging Technologies, 4,* 116–122.

Ebadi Jamkhaneh, M., Davoodi, M. R., & Ebadi Jamkhaneh, J. (2017). Assessment of the ball joint behavior under combine loading. *IQBQ, 17*(5), 149–159. **(in Persian)**.

El-Sheikh, A. I. (1993). Numerical analysis of space trusses with flexible member-end joints. *International Journal of Space Structures, 8*(3), 189–197.

Fan, F., Ma, H., Chen, G., & Shen, S. (2012). Experimental study of semi-rigid joint systems subjected to bending with and without axial force. *Journal of Constructional Steel Research, 68*(1), 126–137.

Fathelbab, F. A. (1987). *The effect of joints on the stability of shallow single layer lattice domes*. Ph.D. Thesis, University of Cambridge.

Fathelbab, F. A. (1993). Tangent stiffness matrix for space frame members with both member and joint imperfections. In G. A. R. Parke & C. M. Howard (Eds.) *Space structure 4. Conference* (pp. 1323–1333). Guildford: Th. Telford Publ.

Ghasemi, M. (2007). *Experimental study of force-displacement relationship pf MERO connection system and investigation of its effect on double layers space structures behavior*. Master thesis, Babol University of Technology, Babol, Iran **(in Persian)**.

Ghasemi, M., Davoodi, M. R., & Mostafavian, S. A. (2010). Tensile stiffness of MERO-type connector regarding bolt tightness. *Journal of Applied Science, 10*(9), 724–730.

Girão Coelho, A. M., Sim˜oes da Silva, L., & Bijlaard, F. S. K. (2006). Ductility analysis of bolted extended end plate beam-to-column connections in the framework of the component method. *Steel and Composite Structures, 6*(1), 33–53.

Guo, X., Huang, Z., Xiong, Z., Yang, S., & Peng, L. (2016a). Numerical studies on behaviour of bolted ball-cylinder joint under axial force. *Steel and Composite Structures, 20*(6), 1323–1343.

Guo, X., Huang, Z., Xiong, Z., Yang, S., & Peng, L. (2016b). Experimental studies on behaviour of bolted ball-cylinder joints under axial force. *Steel and Composite Structures, 21*(1), 137–156.

Maalek, S. (1999). Structural assessment and quality control procedures for the Homa Aircraft Hangar No. 3. *International Journal of Space Structures, 14*(3), 167–184.

Mathurin, F., Guillot, J., Stéphan, P., & Daidié, A. (2009). 3D finite element modeling of an assembly process with thread forming screw. *Journal of Manufacturing Science and Engineering, 131,* 041015.

See, T., & McConnel, R. E. (1986). Large displacement elastic buckling of space structures. *Journal of Structural Engineering, 112*(5), 1052–1069.

Serway, R. A., & Beichner, R. J. (2000). *Physics for scientists and engineers* (5th ed.). Orlando: Saunders College Publishing.

Ueki, T., Matsushita, F., Shibata, R., & Kato, S. (1993). Design procedure for large single-layer latticed domes. *Space Structures, 4*(1), 237–246.

Vaseghi Amiri, J., & Davoodi, M. R. (2002). Modeling of semi-rigid behavior of MERO jointing system. *Space Structures, 5*(1), 309–316.

Yuan, H., Liu, H., Ren, X., Zhang, X., Ai, D., & Luo, Y. (2019). The bearing performance of the bolt-sphere joints with stochastic pitting corrosion damage. *Journal of Constructional Steel Research, 160,* 359–373.

Zeng, Q., Guo, X., Huang, Z., & Zong, S. (2019). Uniaxial compression bearing capacity of bolted ball-cylinder joint. *Engineering Structures, 183,* 976–986.